Received: 11 December 2019 | Revised: 20 April 2020 | Accepted: 9 May 2020

DOI: 10.1002/jbm.b.34639

ORIGINAL RESEARCH REPORT

Society For Biomaterials | WILEY

CD68+ macrophages as crucial components of the foreign body reaction demonstrate an unconventional pattern of functional markers quantified by analysis with double fluorescence staining

Uwe Klinge[1] | Axel Dievernich[1] | Rene Tolba[2] | Bernd Klosterhalfen[3] | Luke Davies[4]

[1]Department of General, Visceral and Transplant Surgery, University Hospital RWTH Aachen, Aachen, Germany

[2]Institute for Laboratory Animal Science and Experimental Surgery, University Hospital RWTH Aachen, Aachen, Germany

[3]Institute for Pathology at the Düren Hospital, Düren, Germany

[4]Division of Infection and Immunity, Cardiff University, Cardiff, UK

Correspondence
Uwe Klinge, Department of General, Visceral and Transplant Surgery, University Hospital RWTH Aachen, Pauwelsstraße 30, 52074 Aachen, Germany.
Email: uklinge@ukaachen.de

Funding information
Federal Ministry of Education and Research, Germany, Grant/Award Number: FKZ 13GW0108B; Welcome Trust, Grant/Award Number: 103973/Z/14/Z

Abstract

Implants like meshes for the reinforcement of tissues implement the formation of a persistent inflammation with an ambient fibrotic reaction. In the inflammatory infiltrate several distinct cell types have been identified, but CD68+ macrophages are supposed to be most important. To investigate the collaboration among the various cell types within the infiltrate we performed at explanted meshes from humans double fluorescence staining with CD68 as a constant marker and a variety of other antibodies as the second marker. The list of second markers includes lymphocytes (CD3, CD4, CD8, CD16, CD56, FoxP3, and CD11b) stem cells (CD34), leucocytes (CD45, CD15), macrophages (CD86, CD105, CD163, and CD206); deposition of EC matrix (collagen-I, collagen-III, MMP2, and MMP8); Ki67 as a marker for proliferation; and the tyrosine-protein kinase receptor AXL. The present study demonstrates within the inflammatory infiltrate the abundant capability of CD68+ cells to co-express a huge variety of other markers, including those of lymphocytes, varying between 5 and 83% of investigated cells. The observation of co-staining was not restricted to a specific polymer but was seen with polypropylene fibers as well as with fibers made of polyvinylidene fluoride, although with differences in co-expression rates. The persisting variability of these cells without the functional reduction toward differentiated mature cell types may favor the lack of healing at the interface of meshes.

KEYWORDS

fluorescence microscopy, foreign body reaction, lymphocyte, macrophage, mesh

1 | INTRODUCTION

Millions of patients are currently treated by mesh implants for the treatment of hernias, pelvic floor weaknesses, vascular deficits, and other disorders reinforcing tissues. However, integration of the device

Uwe Klinge and Axel Dievernich contributed equally to this study.

within fat, muscle, or fibrous tissues is hampered by chronic inflammation with concomitant fibrotic scar formation. This state-of-affairs favors a stiff-scar plate, nerve entrapments, chronic pain, migration, or erosion of adjacent structures (Glazener et al., 2017). The long-term safety of medical devices such as surgical meshes (Klosterhalfen & Klinge, 2013; Nolfi et al., 2016) or breast implants (Bachour et al., 2018) is decisively determined by the reaction of the host at the interface, in most cases forming a foreign body granuloma (FBG), with adjacent mononuclear inflammatory infiltrate and a surrounding fibrotic capsule (Figure 1). For decades, macrophages have been considered as the dominant immune cell subset in this chronic inflammation, usually being identified by their morphology and surface markers, such as CD68, CD86, or CD206 (Kunisch et al., 2004). Macrophages display tissue-specific diversity and a plastic ability to change their phenotype for production of cytokines to promote either chronic inflammation or wound healing (Krzyszczyk, Schloss, Palmer, & Berthiaume, 2018). These phenotypes are governed primarily by the local tissue microenvironment (Davies & Taylor, 2015). To characterize the inflammatory infiltrate in more detail, in 2014 we had studied the expression of various markers in the FBG of meshes by immunohistochemistry (Klinge, Dietz, Fet, & Klosterhalfen, 2014). The abundant expression of CD68, CD45, as well as CD8 within the FBG, suggested the possibility that macrophages alone may not be playing the decisive part. Consistently, Tennyson et al. (2018) analyzed tissue reactions to explanted pelvic floor meshes and confirmed the presence of abundant lymphocytes, for example, CD4+ helper T cells, CD8+ cytotoxic T cells, or FOXP3+ regulatory T cells. Furthermore, our observation of widespread positive staining of different markers suggested that cells may co-express some of them.

Surface markers such as CD68, CD4, or CD8 are generally considered to reliably separate macrophages from lymphocytes. Although flow cytometry experiments already have shown in some cell clusters dual expression of CD68, and of CD4 or CD8 (Adamthwaite & Cooley, 1994; Hameed, Hruban, Gage, Pettis, & Fox 3rd., 1994; Kunisch et al., 2004; Murray et al., 2014; Wang, Windgassen, & Papoutsakis, 2008; Zaynagetdinov et al., 2013), however, whether or not such co-expression of macrophage and lymphocyte lineage markers in the same cell are relevant in situ is unclear.

In the present study at explants from human patients, we tested in the cells of the inflammatory infiltrate the expression of various cell markers by double fluorescence staining to identify cell types other than CD68+ and to look for possible co-expression in CD68+ cells. The list of second markers include CD3 (lymphocytes), CD4 (T-helper), CD8 (cytotoxic T), CD16 (NK-cell), CD56 (NK-cell), FoxP3 (Treg), CD11b (DC), CD34 (stem cell), CD45 (leucocytes), CD15 (granulocytes), macrophages CD86 (pro-inflammatory M1), CD105 (activated, part of the TGF-receptor complex), CD163 (part of the scavenger receptor complex), CD206 (anti-inflammatory M2); deposition of EC matrix: collagen-I, collagen-III, MMP2, MMP8; Ki67 served as marker for proliferation; and AXL (tyrosine-protein kinase receptor) as inhibitor of the innate immune response. Furthermore, we looked for the proliferative activity of CD68+ cells as indicative for a local self-renewal.

2 | MATERIALS AND METHODS

We analyzed 15 meshes made of polypropylene (PP), and five made of polyvinylidene fluoride (PVDF), which all had been used for abdominal wall hernia repair in humans, and were excised between 1999 and 2017 (approval by ethic committee EK 239/19). All the meshes of this study are made of monofilaments, either of PP or PVDF. In some of the samples the material could be clearly identified: seven large pore Ultrapro®, two Ventralex® with a layer of PTFE, two small pore plugs, one Vypro®, one Proceed®, and five Dynamesh®-IPOM. In two others we cannot be sure about the specific material used, other than a monofilament is used. Human tissue samples of the spleen, liver, lymph node, and tonsil without gross pathology served as healthy control tissue. All samples were embedded in paraffin for subsequent investigations.

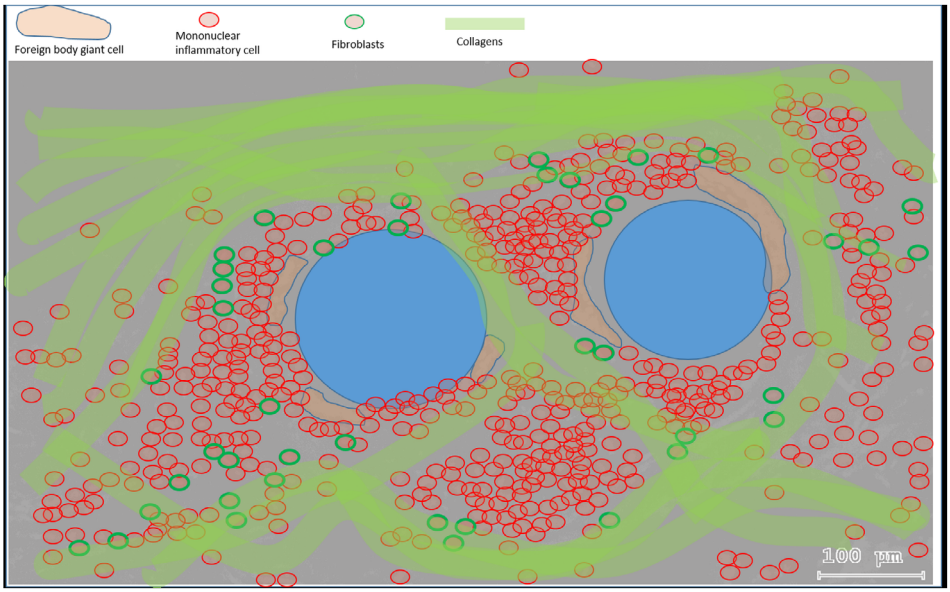

FIGURE 1 Foreign body reaction: Foreign body giant cells, an inner inflammatory infiltrate of mononuclear cells with expression of various markers (e.g. 25.7% CD68+), and an outer fibrotic capsule with collagen deposits around two fibers, in contrast to collagen deposits in scar tissue without this accumulation of inflammatory cells

Prior to immunofluorescence staining, mesh samples were checked for the presence of mesh and FBGs by hematoxylin and eosin (supplemental Figure 1) as well as diaminobenzidine immunohistochemical staining. All mesh samples showed the typical foreign body reaction around the mesh fibers with an inner layer of inflammatory infiltrate, followed by an outer fibrotic layer. Most specimens showed a varying number of lymphocytes and foreign body giant cells (FBGCs), as well as small vessels at the mesh–tissue interface. Eight of 15 mesh explants made of PP were explanted due to hernia recurrence and three because of low-grade infection, defined by an accumulation of at least 23 polymorphonuclear cells per high power field. The tissue reaction to PDVF meshes was quite similar to PP meshes but less pronounced. The granulomas were smaller in PDVF compared to PP, particularly their fibrotic tissue layer; and the inflammatory infiltrate consists of smaller numbers of lymphocytes and FBGCs.

3 | IMMUNOFLUORESCENT STAINING

3.1 | General

All steps were performed at room temperature. Serial 2 μm sections of each specimen were double-labeled with CD68 as the first marker in combination with various other markers (Table 1). CD68 was always stained with fluorescein isothiocyanate (FITC), and the second marker with cyanine-5 (Cy5). All antibodies used were monoclonal and diluted with Antibody Diluent (with Background Reducing Components, Dako, Germany). Secondary antibodies were applied with ImmPRESS™ HRP (Peroxidase) Polymer Detection Kit (Vector, Laboratories, USA). Fluorochromes were diluted with 1× Plus Amplification Diluent (PerkinElmer, USA).

3.2 | Protocol

Tissue sections were deparaffinized with xylene, rehydrated through graded alcohol and Milli-Q, before incubation in 3.5% formalin for 10 min. Sections were then placed in a cuvette filled with Milli-Q and pH 6 citrate buffer (1:10) and treated with a Decloaking Chamber™ (Biocare Medical, USA) for 10 min at 110°C. Afterward, sections were washed with Milli-Q and TBST Tris (Buffered Saline with Tween 20, Dako) and cooled. Nonspecific binding was blocked by incubation with Antibody Diluent for 10 min.

These steps were followed by incubation with the primary antibody of the first marker. After incubation, sections were rinsed in TBST Tris and incubated with the secondary antibody for 20 min, before applying FITC-staining with the Opal™ 520 Reagent Pack (1:100, PerkinElmer) for 10 min. Sections were then washed with TBST Tris and placed in a cuvette filled with AR6 Buffer (PerkinElmer)

TABLE 1 List of monoclonal antibodies used.

Antibody	Clone	Dilution	Incubation time	Manufacturer
CD15	FUT4/815	1:600	Overnight	Abcam
CD34	QBEND-10	1:2,500	Overnight	Abcam
MMP8	EP1252Y	1:300	Overnight	Abcam
CD16	c127	1:50	Overnight	Acris
CD206	15–2	1:200	30 min	Acris
TCR γ/δ	B1	1:50	30 min	BioLegend
CD163	5C6 FAT	1:800	Overnight	BMA Biomedicals
CD3	F7.2.38	1:1,000	30 min	Dako
CD4	4B12	1:500	30 min	Dako
CD8	CD8/144B	1:500	30 min	Dako
CD45	2B11 + PD7/26	1:2,000	30 min	Dako
CD56	123C3	1:200	30 min	Dako
CD68	KP1	1:6,000	30 min	Dako
CD105	SN6h	1:25	Overnight	Dako
Ki67	MIB-1	1:500	30 min	Dako
FoxP3	PCH101	1:250	30 min	eBioscience
AXL	7E10	1:800	30 min	MyBioSource
CD86	BU63	1:200	Overnight	Novus Biologicals
CD11b	OTI12C10	1:2,000	30 min	OriGene
Collagen-I	5D8-G9	1:125	Overnight	ThermoFisher
Collagen-III	FH-7A	1:200	30 min	ThermoFisher
MMP2	CA-4001 or CA719E3C	1:300	Overnight	ThermoFisher

Note: Monoclonal antibodies used in this study are sorted alphabetically by the manufacturer. Additional information given are type of clone, dilution, and incubation time.

and Milli-Q (1:10). The cuvette was microwave treated for 3 min at 385 W reaching a maximal temperature of 92°C and 15 min at 120 W reaching a maximal temperature of 90°C, before being cooled with cold water. Sections were removed and rinsed with Milli-Q, before incubation with TBST Tris overnight.

The second marker was applied on the following day. After applying the primary and secondary antibodies of the second marker, sections were Cy5-stained with the TSA™-Plus Cyanine 5 System (1:50, PerkinElmer). Sections were then rinsed in Milli-Q and counterstained with TBST Tris diluted Spectral DAPI (1:12.5, PerkinElmer) for nuclei. Finally, all tissue sections were mounted with VECTRASHIELD® HardSet™ Antifade Mounting Medium (Vector) and coverslipped.

3.3 | Analysis of the fluorescence images/stainings

Fluorescence imaging was performed with an Axio Imager 2 microscope (20×, Zeiss, Germany) and the TissueFAXS PLUS system (TissueGnostics, Austria). Images were processed and quantitatively analyzed with StrataQuest Analysis Software (v6, TissueGnostics). Optimized DAPI images were used to detect and segment nuclei (Figure 2). Nuclei areas were used to measure the mean staining intensities on FITC- and Cy5-shades in selected 1 mm^2 circular regions of interest (ROIs) that were placed around mesh fibers, each including about 2,000–5,000 nuclei (Figure 3). About 11 (median; range: 4–35) ROIs were analyzed in each sample for all stainings to represent the FBG. The area of the entire sample without the area of the ROIs was considered mesh-scar tissue. We recorded the total number of nuclei, as well as the percentages of $FITC^+$ ($CD68^+$), $Cy5^+$ (second $marker^+$), and the double-positive $FITC^+Cy5^+$ (CD68+ and second marker+) cells.

Additionally, controls without primary antibody and controls with isotype antibodies were performed, the later with all dilutions and incubation times (Figure 4). With a cut-off value of 100 for the mean intensity in the nuclear area on average less than 2% of false-positive cells were detected (Table 2).

3.4 | Statistical analysis

Calculations were done with MATLAB® 9.1 and Image Processing Toolbox 9.5 (The MathWorks, USA). Statistical analysis was performed using Statistical Package for Social Sciences software (SPSS® v23, IBM, USA). Differences between groups and statistical p were assessed by the nonparametric Mann–Whitney U test. The raw data required to reproduce these findings are available on request from the authors.

4 | RESULTS

In different healthy human control tissues we always found some cells stained positive for CD68 as well as for $CD45^+$, $CD8^+$, $CD4^+$, or $CD3^+$, but cells that co-expressed $CD68^+$ $CD45^+$, $CD68^+$ $CD8^+$, $CD68^+$ $CD4^+$, and $CD68^+$ $CD3^+$ were almost absent (<2% of all cells) (Figure 5;

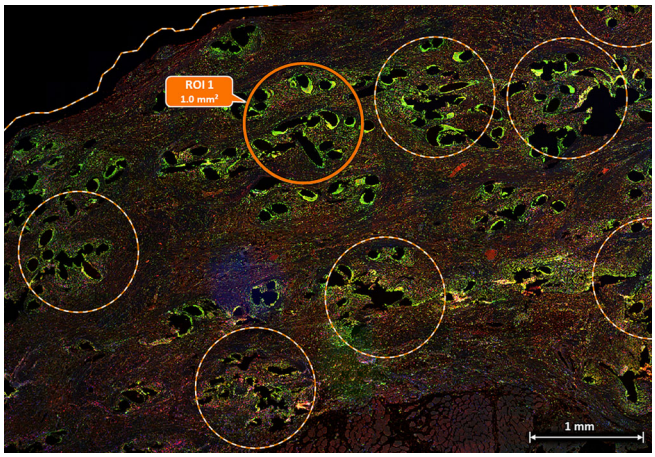

FIGURE 3 Regions of interest (ROI) selection. Tissue section of a human mesh explant with selected circular ROI. Each ROI has an area of 1 mm^2, contains at least one mesh fiber, and 2,000–5,000 nuclei

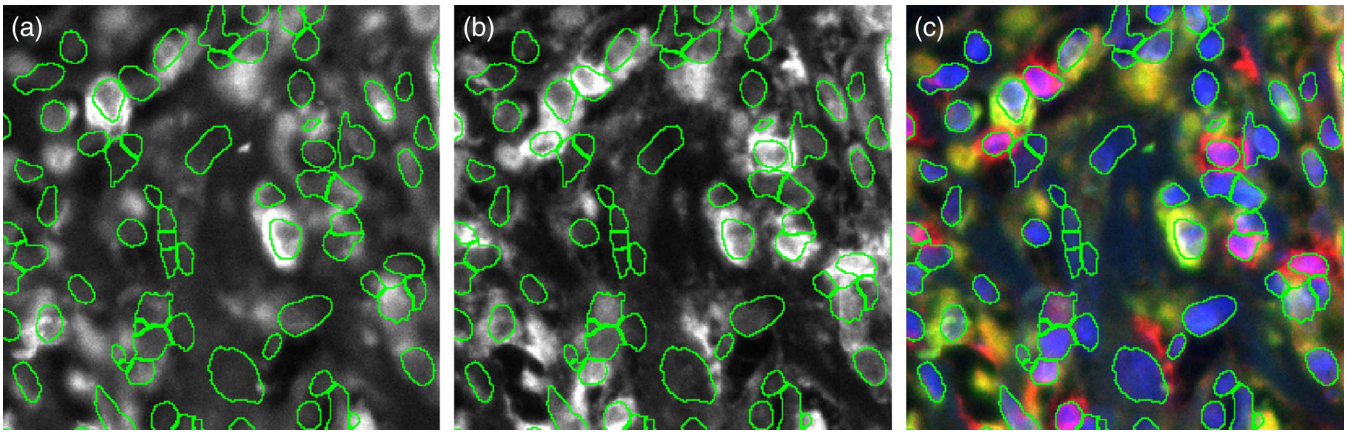

FIGURE 2 Nuclei outlines on grayscale marker images and superimposed color image. (a) Grayscale image of CD68 stained with fluorescein isothiocyanate (FITC). (b) Grayscale image of CD8 stained with. (c) Merge of DAPI colored in blue, CD68 colored in green, and CD8 colored in red. Co-expressing CD68 + CD8+ cells are colored yellow. All images have been superimposed with the contours of the cell nuclei in solid green color

Table 3). In mesh-scar tissue, 19% of all cells were CD68$^+$, and about 10% were positive for the lymphocyte markers CD3, CD4, or CD8. However, co-expression of CD68 with CD45, CD3, CD4, or CD8 still was rare (2.8–4.8% of all cells). In contrast, in the area of the FBG around PP meshes, all these markers were seen abundantly, and co-staining with CD68 was frequently found. Between 30 and 50% of the CD68$^+$ cells were positive for a second marker, and half of the cells being positive for CD45$^+$, CD8$^+$, CD4$^+$, and CD3$^+$ were simultaneously positive for CD68$^+$ (Figure 6).

To test whether or not this dual-labeling was restricted to CD45, CD8, CD4, and CD3 in PP meshes we expanded our analysis to a mesh of another polymer and to further markers, which are considered to specify distinct cell types or reflect functional properties such as deposition of collagen, including CD86 (M1), CD163 (scavenger receptor on macrophages, an innate immune sensor for bacteria), CD206 (M2), CD105 (part of the TGF-β receptor complex, activated macrophages), CD16 (NK cell marker I), CD56 (NK cell marker II), CD11b (Mac-1, dendritic cell marker), TCR γ/δ, CD34 (stem cell), CD15 granulocytes, AXL, collagen-I and collagen-III, MMP2 and MMP8. For all these markers, considerable numbers of single positive-labeled cells were observed in the FBG of meshes made of both PP or PVDF, ranging from 2.2% CD86$^+$ cells to 54.6% AXL$^+$ cells around PP meshes, and from 1.2% CD86$^+$ cells to 62.3% collagen-III$^+$ deposits around PVDF meshes, detected at PP mesh ROIs with mean 3,186 nuclei, PVDF mesh ROIs with mean 2,519 nuclei, respectively (Figure 7; Table 4). While positively stained cells were mainly observed at the mesh–tissue interface for most markers, this was not the case for CD34, CD86, and MMP8, which usually were located outside the FBG. FBGCs were positive for most markers, though showing strong heterogeneous staining patterns even within their multinucleated cell bodies.

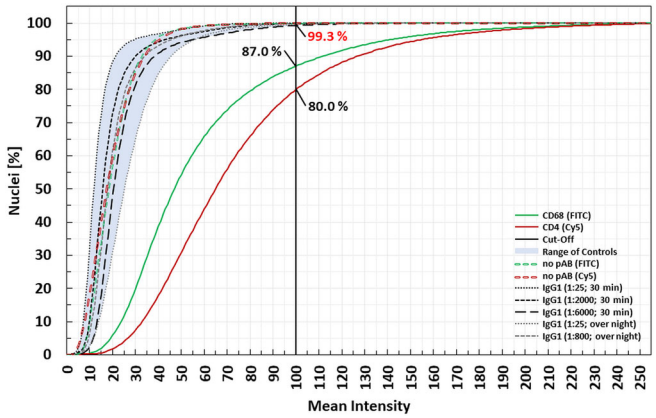

FIGURE 4 Cumulative mean intensity distributions do not indicate distinct subgroups. Cumulative mean intensity distributions for all markers (e.g. CD68 labeled with fluorescein isothiocyanate (FITC) and CD4 labeled with Cy5) at human mesh explants never showed any s-shape or step, which would have reflected a distinct cluster of positive-labeled cells with higher intensities. Instead, the continuous smooth rise confirms the presence of a continuum and a strong cellular heterogeneity, not indicating a distinct cut-off to differentiate between positive- and negative-labeled cells. The curves of controls are strongly left-shifted; the cut-off value of 100 detects true positive cells with high intensities without including many false positives as can be seen by the lowest percentage of 99.3% for controls (positive predictive value >99%)

Markers with high numbers of positive-labeled cells within the inflammatory infiltrate usually showed higher cell densities closer to the fibers, with no distinct zones that separate positive- and negative-labeling. Most of these markers even displayed a local gradient with continuously decreasing mean intensities with increasing distance from the mesh fibers (Figure 8).

All markers tested showed substantial **co-expression** with CD68$^+$ within the inflammatory infiltrate of the FBG, ranging from 5% for CD68$^+$CD86+ to 83% for CD68$^+$AXL$^+$ cells, mainly preferential close to the mesh fibers (Figures 9 and 10a–d; Table 4).

To study whether or not the inflammatory infiltrate of the FBG derives from proliferating cells, we looked for the expression of Ki67 at meshes, which at PP was found on average in 5.8% of the cells. Furthermore, we identified 13.1% double-labeled CD68 + Ki67+ cells, and 54.4% of Ki67+ cells co-expressed CD68, again mainly located in the vicinity of the mesh fibers (Figure 11; Table 5).

The values for PVDF meshes were quite similar with 7.1% Ki67+, and 13.3% CD68 + Ki67+, and 60.7% of Ki67+ cells co-expressed CD68, respectively.

5 | DISCUSSION

Mesh-related complications are usually attributed to the foreign body reaction characterized by chronic fibrotic inflammation at the mesh boundary. Inflammation is governed by the types of immune cells on

TABLE 2 Calculation of the positive predictive value (PPV).

	PPV			
Marker	Cut-off 100 (%)	Cut-off 80 (%)	Cut-off 60 (%)	Cut-off 40 (%)
CD68 (FITC)	*99.8*	99.7	98.8	92.4
CD3 (Cy5)	*99.2*	97.6	94.8	80.3

Note: PPV = (true positives)/(true positives + false positives) × 100%.
Note: True positives = Number of cells with a mean staining intensity above the cut-off value seen after full staining with a specific monoclonal antibody.
Note: False positives = cells with a mean staining intensity above the cut-off value seen in controls without primary antibody.
Note: Calculation of the PPV for different cut-off values for CD68 (FITC) and CD3 (Cy5). A cut-off value >100 for the mean staining intensities yields PPVs >99%. Decreasing the cut-off value results in higher rates of falsely positive detected cells.

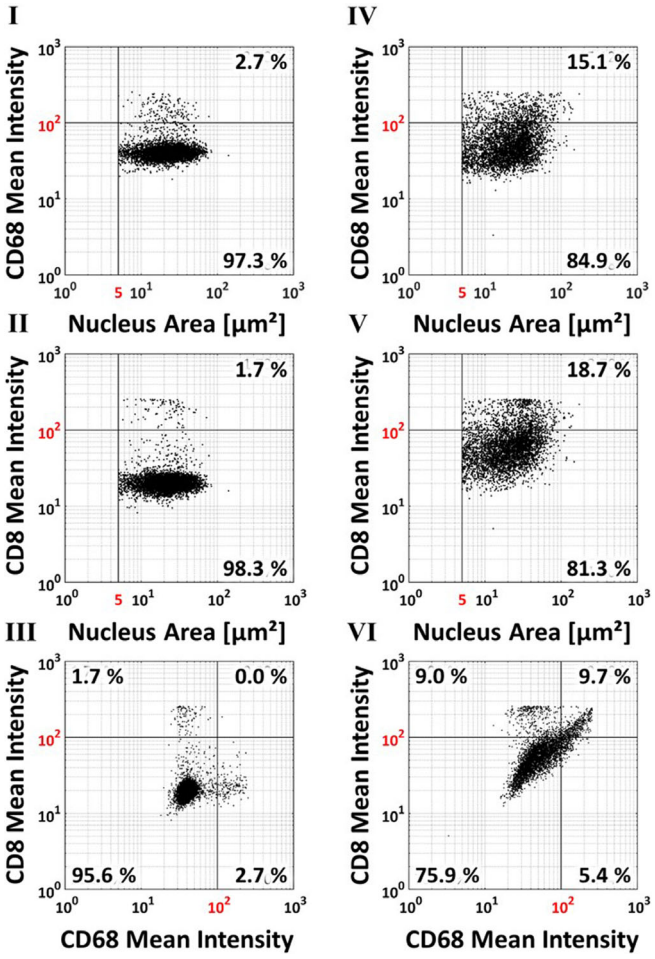

FIGURE 5 Comparison of healthy human liver tissue with a foreign body granuloma of a human polypropylene (PP) mesh explant. Scatterplots of the mean staining intensities from a healthy human liver sample (left column, I–III), and of a human PP mesh explant (right column, IV–V). The solid black lines mark the mean intensity cut-off value 100 and the nucleus area cut-off value 5. Double positive-labeled cells are in the upper right quadrants of scatter plots III and VI. Percentages of cells in each quadrant are displayed in the outer corners

site. In the present study, we demonstrated that the inflammatory infiltrate at explanted meshes from human patients displays extreme heterogeneity and is quite dissimilar to that of a healing wound (scar tissue). The simultaneous presence of these markers is indicative of a spatial chronic inflammatory microenvironment primarily localized around the foreign body and reflects the complex activation of these cells possibly triggering their inherent inability for definitive healing.

When examined, the majority of antibody labeling was present at the interface to clinical meshes, reflecting active recruitment. In situ quantification of the staining intensity within the FBG revealed a multi-marker pattern, indicating the high level of immune cell activation, as the majority of markers are known to up-regulate protein expression after inflammatory signaling cascades (Heymann et al., 2019). The local gradient with declining intensities in relation to the distance of the foreign body underlines the impact of the local conditions and questions the ability of in vitro experiments to reflect this real-world scenario.

We identified that $CD68^+$ cells co-express a variety of surface markers, which usually are linked to other immune cells. Most of the $CD68^+$ cells are considered to be macrophages, and have been previously reported to show expression of CD45 (leucocytes), CD86 (pro-inflammatory M1), CD206 (anti-inflammatory M2), CD16 (neutrophil/natural killer cell marker), CD56 (natural killer cell marker I), CD11b (part of the MAC-1 complement receptor), CD105 (part of the TGF beta receptor complex, activated macrophages), or CD163 (scavenger receptor on macrophages, an innate immune sensor for bacteria) (Pilling, Fan, Huang, Kaul, & Gomer, 2009). However, we were surprised that almost half of the $CD68^+$ cells co-express lymphocytic markers such as CD3, CD4 (helper T-cells), or CD8 (cytotoxic T-cells). Gamma-delta T-cells can sometimes display macrophage morphology (Wu et al., 2009); however, we identified only rare expression of T-cell receptor γ/δ.

The enormous level of co-expression seen within the local inflammatory cells within the FBG can reflect the extended capabilities of both macrophages and lymphocytes if such a strict distinction is still useful. Perhaps these data just restore the historical idea of the presence of multipotent inflammatory or wound healing cells, considered to be histiocytes by Aschoff (Yona & Gordon, 2015), macrophages by Metschnikoff (Cavaillon, 2011), fibrocytes by Bucala (Bucala, Spiegel, Chesney, Hogan, & Cerami, 1994), resting wandering cells by von Recklinghausen (Guilliams et al., 2014), polyblasts by Maximow (Jablonski & Meyer, 1938), or generally summarized as cells of the macrophage system (Murray et al., 2014).

The explanation for this extreme heterogeneity could be the radical adaptation of the immune system to eliminate an indigestible foreign object. Such a reaction is commonly identified in parasite infections, where the macrophages fuse and form giant cells (Ruckerl & Allen, 2014). An identical phenomenon has been observed at the interface to our meshes and has been reported even between T cells and macrophages in HIV infection (Bracq et al., 2017). However, multicell fusion cannot explain the heterogeneity we observe at the mesh boundary, as the cells we identify are widely mononuclear. An alternative mechanism could be emergency hematopoiesis, such as that occurring in cancer and infections, where immature immune cells are recruited from the bone marrow and display stem-like properties (Boettcher & Manz, 2017). The level of multipotency may allow expression of normally lineage-restricted genes and proliferation at the site of the implant. Our data revealed that the majority of $Ki67^+$ cells (indicating proliferation potential) were also positive for CD68, confirming these CD68 + Ki67+ cells are not terminally differentiated and can proliferate in situ rather than relying on newly recruited bone marrow monocytes, as has been observed in monocyte-derived macrophages in mice (Davies, Jenkins, Allen, & Taylor, 2013). This state-of-affairs may explain the level of cross-lineage heterogeneity we observe, though a more thorough examination by methods of lineage tracing as well as extended multiplex stainings will help to unravel the underlying mechanism (Baron & van Oudenaarden, 2019).

TABLE 3 Co-expression of cells in healthy human tissues and human mesh explants.

Staining	Spleen (645,513 to 742,442 nuclei)	Liver (34,079 to 43,125 nuclei)	Lymph node (199,598 to 267,760 nuclei)	Tonsil (409,571 to 784,518 nuclei)	Mesh-scar (8,876 to 507,584 nuclei)	FBG (2,814 to 5,003 nuclei)
CD68+	1.2–3.1	2.6–3.3	0.5–2.8	0.1–0.4	18.6 (1.7)	28.7 (1.7)*
CD45+	14.8	10.7	0.7	0.6	7.1 (1.2)	19.1 (1.8)*
CD8+	8.1	5.3	2.4	17.8	10.9 (2.3)	18.6 (2.8)*
CD4+	5.2	8.7	13.9	5.3	10.0 (1.7)	21.0 (3.2)*
CD3+	19.0	5.8	10.8	10.6	10.4 (1.9)	20.2 (2.6)*
CD68 + CD45+	0.3	0.9	0.0	0.0	2.9 (0.5)	10.2 (1.5)*
CD68 + CD8+	0.0	0.1	0.0	0.0	3.5 (1.2)	8.6 (1.8)*
CD68 + CD4+	0.3	0.9	0.9	0.1	4.8 (1.3)	13.1 (2.4)*
CD68 + CD3+	0.1	0.1	0.0	0.0	4.4 (1.3)	9.8 (1.8)*
CD4 + CD8+	1.6	1.9	0.1	1.6	3.5 (0.6)	7.8 (1.2)*

Note: Percentages of single and double "positive" cells with a mean intensity >100 in healthy human tissues (spleen, liver, lymph node, and tonsil), and in 15 human mesh explants (foreign body granuloma [FBG], and surrounding scar tissue [mesh-scar]). Data are presented as mean (*SE*). Statistical significance between FBG and Scar was determined by Mann–Whitney *U* test. *p*-values <.05 were considered to be significant and marked by *.

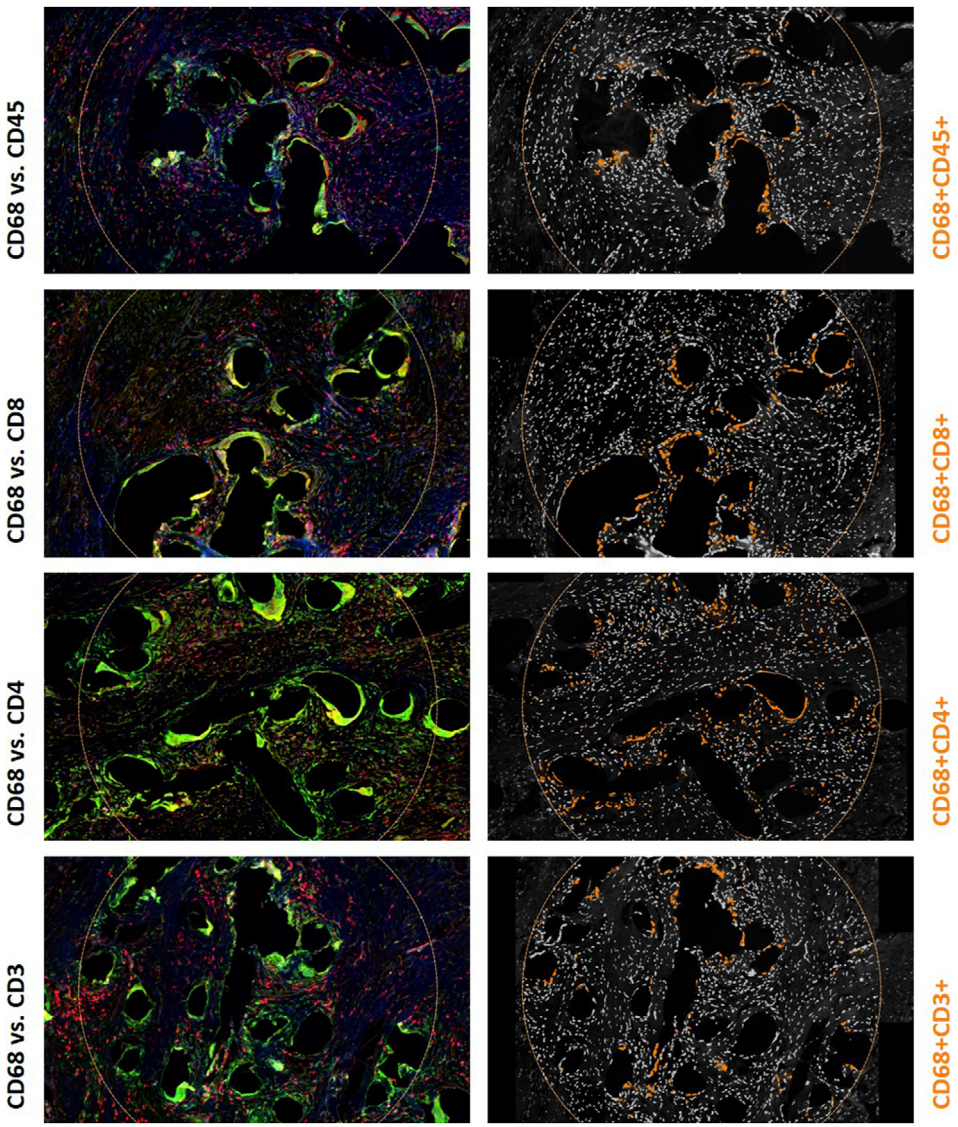

FIGURE 6 Co-expression of cells within the inflammatory infiltrate of the foreign body granuloma. Double immunofluorescence stainings of human mesh explants for CD68 stained with fluorescein isothiocyanate (FITC) (green) and CD45, CD8, CD4, or CD3 stained with Cy5 (red) on the left as well as nuclei images on the right. Nuclei co-expressing both markers are colored in orange. Cells with a mean staining intensity >100 are considered to be "positive"

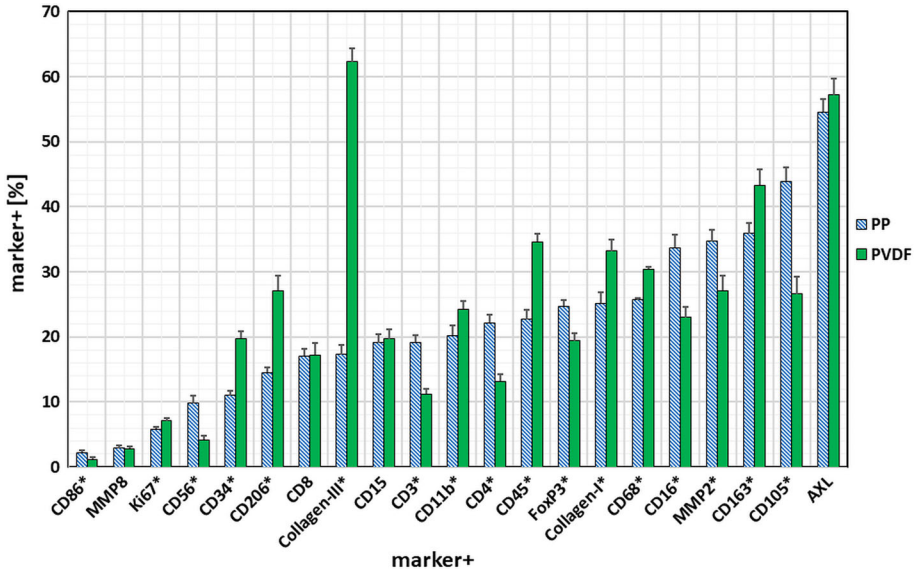

FIGURE 7 Staining patterns in the foreign body granuloma (FBG) around polypropylene (PP) and polyvinylidene fluoride (PVDF) meshes. Percentages of positive-labeled cells in the FBG around both materials (1,819 PP-ROIs and 1,305 PVDF-ROIs). Data are represented as mean with whiskers (±*SE*). Statistical significance between PP and PVDF meshes was determined by Mann Whitney *U* test. Markers with *p*-values <.05 are marked with *

TABLE 4 Labeling of cells in the inflammatory infiltrate of the foreign body granuloma at seven human PP and five human PVDF mesh explants.

	PP meshes			PVDF meshes		
Marker+	Single positives (marker+)	Double positives (CD68 + marker+)	(CD68 + marker+)/ CD68+	Single positives (marker+)	Double positives (CD68 + marker+)	(CD68 + marker+)/ CD68+
CD68+	25.7 (0.3)	–	–	30.4 (0.3)	–	–
CD3+	**19.2 (1.0)**	**8.3 (0.6)**	**29.9 (1.7)**	**11.2 (0.8)***	**2.6 (0.3)***	**10.0 (1.7)***
CD4+	**22.2 (1.2)**	**14.0 (0.9)**	**47.5 (1.9)**	**13.2 (1.0)***	**7.8 (0.6)***	**32.2 (2.5)***
CD8+	**17.1 (1.0)**	**8.1 (0.6)**	**36.0 (2.3)**	**17.2 (1.8)**	**6.7 (1.0)**	**32.6 (3.5)**
CD11b+	**20.2 (1.5)**	**10.0 (0.9)**	**45.2 (2.6)**	**24.3 (1.2)***	**16.3 (1.0)***	**48.9 (2.3)**
CD15+	**19.1 (1.3)**	**10.6 (0.9)**	**37.6 (2.2)**	**19.7 (1.4)**	**10.9 (0.9)**	**31.1 (2.4)***
CD16+	**33.7 (2.0)**	**12.8 (1.2)**	**52.0 (3.1)**	**23.0 (1.6)***	**8.3 (0.7)***	**33.5 (2.4)***
CD34+	**11.0 (0.7)**	**1.2 (0.1)**	**5.1 (0.8)**	**19.8 (1.0)***	**2.7 (0.3)***	**10.0 (1.2)***
CD45+	**22.7 (1.4)**	**8.1 (0.5)**	**41.3 (2.0)**	**34.6 (1.2)***	**14.6 (1.0)***	**54.1 (2.6)***
CD56+	**9.8 (1.1)**	**5.1 (0.6)**	**25.8 (3.0)**	**4.2 (0.6)***	**3.1 (0.5)***	**11.9 (1.7)***
CD86+	**2.2 (0.3)**	**0.7 (0.1)**	**5.0 (0.8)**	**1.2 (0.3)***	**0.8 (0.2)**	**3.7 (0.8)***
CD105+	**43.9 (2.1)**	**13.5 (0.8)**	**64.2 (2.4)**	**26.6 (2.7)***	**9.5 (1.0)***	**46.0 (4.1)***
CD163+	**35.9 (1.6)**	**11.8 (0.6)**	**71.9 (1.7)**	**43.3 (2.4)***	**25.0 (1.4)***	**75.7 (2.7)***
CD206+	**14.5 (0.8)**	**9.7 (0.5)**	**63.5 (2.5)**	**27.1 (2.3)***	**16.7 (1.1)***	**60.4 (3.3)**
AXL+	**54.6 (2.0)**	**17.9 (0.8)**	**83.1 (1.4)**	**57.2 (2.5)**	**21.8 (1.2)***	**81.3 (2.5)**
Collagen-I+	**25.2 (1.6)**	**10.7 (0.8)**	**60.6 (3.7)**	**33.2 (1.8)***	**24.6 (1.2)***	**64.8 (2.5)**
Collagen-III+	**17.3 (1.5)**	**4.8 (0.5)**	**29.0 (2.2)**	**62.3 (2.0)***	**25.9 (1.1)***	**77.1 (2.1)***
FoxP3+	**24.7 (1.0)**	**9.9 (0.4)**	**42.1 (1.5)**	**19.4 (1.1)***	**10.7 (0.7)**	**34.1 (2.0)***
Ki67+	**5.8 (0.3)**	**3.1 (0.2)**	**13.1 (0.7)**	**7.1 (0.4)***	**7.1 (0.4)***	**13.3 (0.7)**
MMP2+	**34.7 (1.7)**	**22.9 (1.2)**	**57.4 (2.1)**	**27.1 (2.3)***	**18.9 (1.7)***	**46.3 (3.2)***
MMP8+	**2.9 (0.4)**	**1.2 (0.2)**	**3.5 (0.6)**	**2.8 (0.4)**	**0.9 (0.1)**	**2.1 (0.3)***

Note: Percentages of single-positive (marker+), and double-positive (CD68 + marker+) cells in reference to all cells as well as the quotient of double-positive cells to CD68+ cells, meaning the percentage of double positives with reference to CD68+ cells. Data are presented as mean (*SE*). Statistical significance between PP and PVDF meshes was determined by Mann Whitney *U* Test. *p*-values <.05 are marked with *.

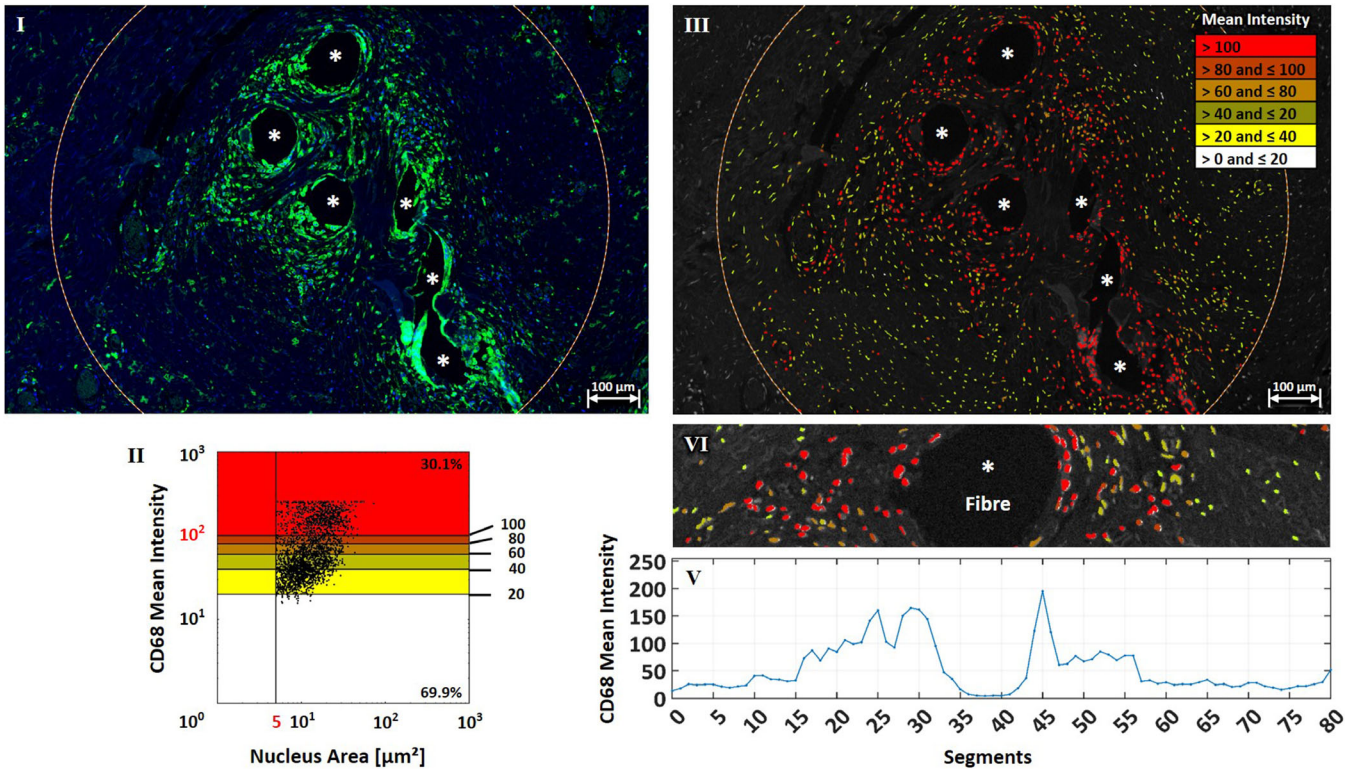

FIGURE 8 Decreasing mean staining intensities with increasing distance from the mesh fibers. (I) Regions of interest (ROI) from a human mesh explant stained for anti-CD68 with fluorescein isothiocyanate (FITC). (II) Scatterplot with nucleus area on the *x*-axis and anti-CD68 mean intensity on the *y*-axis. 30.1% of the cells within the ROI have a mean intensity >100 (red area). Cells with lower mean intensities are clustered in steps of 20. Each cluster has an individual color assigned. (III) Cells colored according to their cluster within the ROI. Cells with high mean intensities are displayed in red and dark orange, whereas cells with low mean intensities are displayed in yellow and white. (IV) Extraction of a rectangular section with a mesh fiber in the center and surrounding inflammatory infiltrate. (V) The mean intensity profile of cells within 10 µm segments shows a decreasing intensity gradient with increasing distance to the foreign body

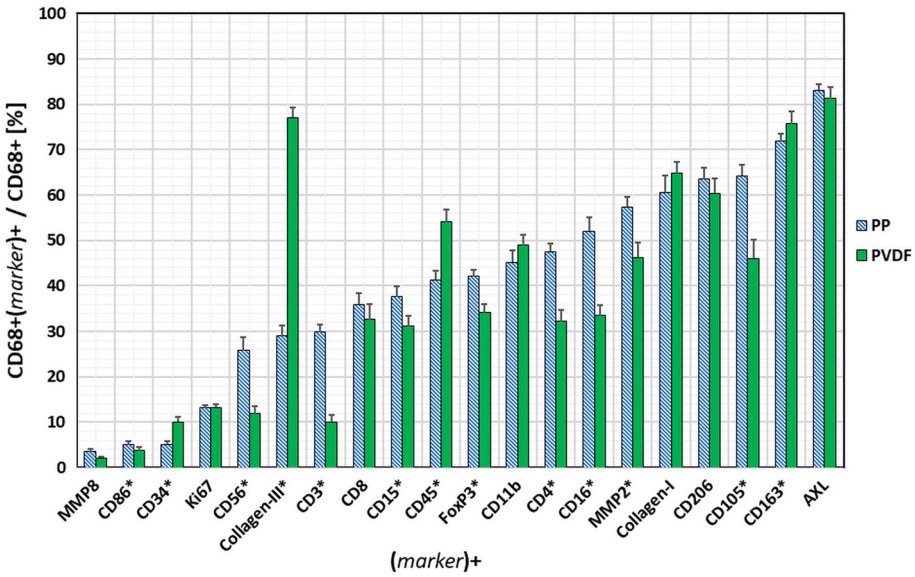

FIGURE 9 Percentages of co-labeling in CD68$^+$ cells in the foreign body granuloma (FBG) around polypropylene (PP) and polyvinylidene fluoride (PVDF) meshes. CD68 was always used as the first marker and labeled with fluorescein isothiocyanate (FITC), whereas secondary markers were always labeled with Cy5. The *y*-axis displays the percentages of double positive-labeled cells in relation to the CD68$^+$ cells in the foreign body granuloma. Data are represented as mean with whiskers (±*SE*). Statistically significant differences between PP and PVDF meshes were determined by Mann Whitney *U* test. Co-labeling with *p*-values <.05 are marked with *

In this study, we can demonstrate that the heterogeneity of immune cells is not restricted to meshes made of PP, but is apparent with meshes made of another polymer PVDF, as well, although with differences mainly for the lymphocytic and collagen markers.

Considering the many problems recorded after the use of meshes to reinforce tissues, it is the persistent local reaction, which underlies the majority of these. The host tissue is not able to effectively seal the foreign body in a stable wall of defending cells and extracellular

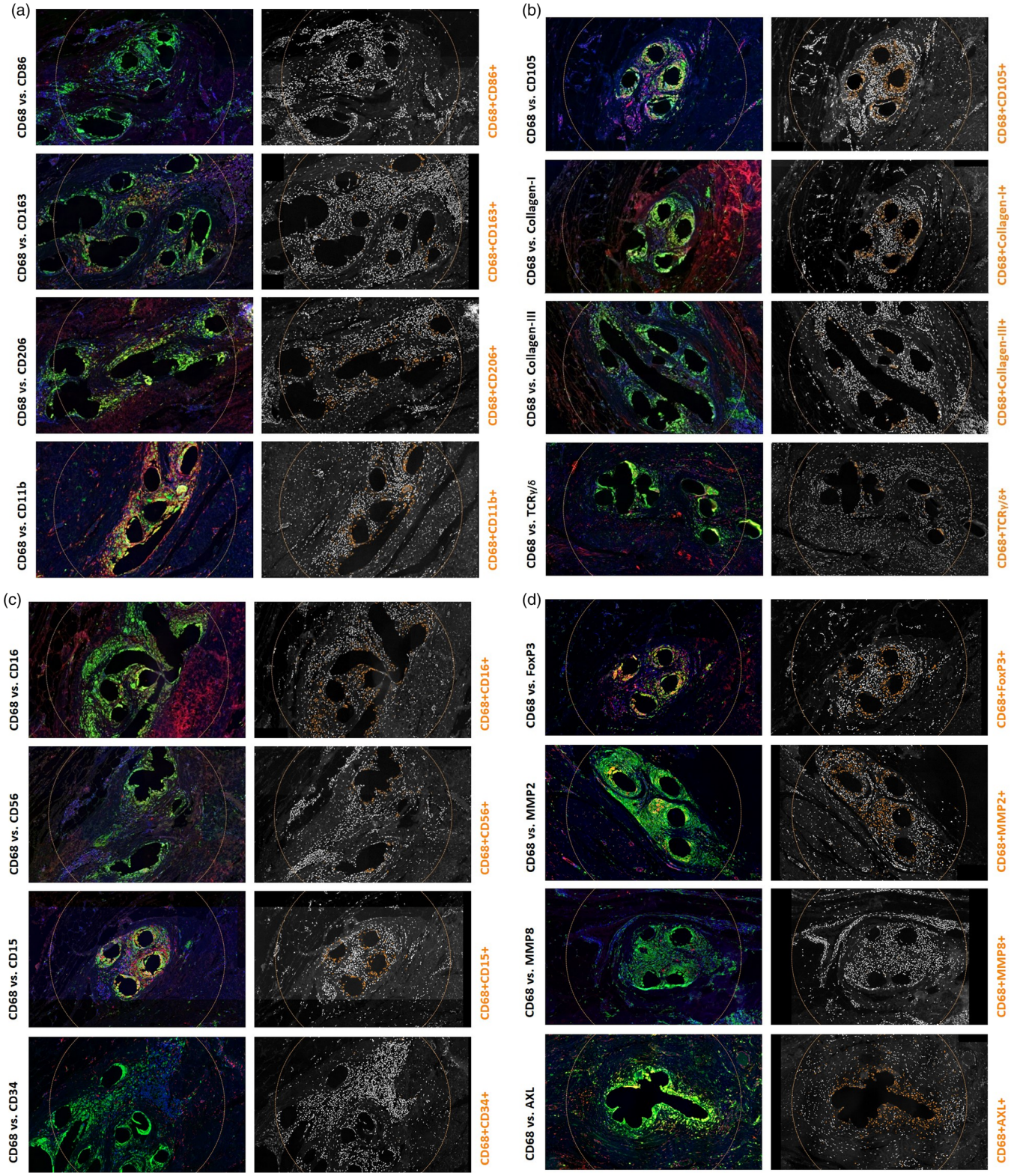

FIGURE 10 Co-expressing cells within the inflammatory infiltrate of the foreign body granuloma. (a) Double immunofluorescence stainings for CD68 stained with fluorescein isothiocyanate (FITC) (green) versus CD86, CD163, CD206, or CD11b stained with Cy5 (red) on the left as well as nuclei images on the right. (b) Double immunofluorescence stainings with FITC (green) versus CD105, Collagen-I, Collagen-II, or TCR γ/δ stained with Cy5 (red) on the left as well as nuclei images on the right. (c) Double immunofluorescence stainings with FITC (green) versus CD16, CD56, CD15, or CD34 stained with Cy5 (red) on the left as well as nuclei images on the right. (d) Double immunofluorescence stainings with FITC (green) versus AXL, MMP8, MMP2, or FoxP3 stained with Cy5 (red) on the left as well as nuclei images on the right. Nuclei co-expressing both markers are colored in orange. Cells with a mean staining intensity >100 are considered to be "positive"

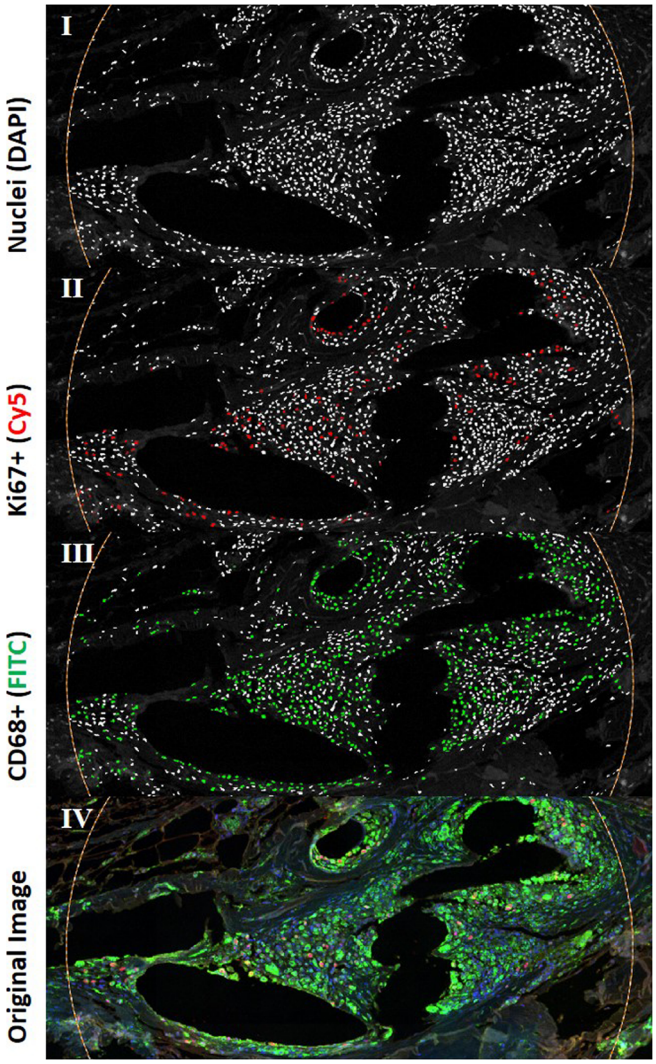

FIGURE 11 Proliferation of cells within the inflammatory infiltrate of the foreign body granuloma. (I) Nuclei stained with DAPI colored in white, (II) nuclei and proliferating Ki67+ cells stained with Cy5 colored in red, (III) nuclei and CD68+ cells stained with fluorescein isothiocyanate (FITC) colored in green, and (IV) overlay of the original shades (DAPI in blue, CD68 in green, and Ki67 in red). Cells were considered to be "positively" stained if their mean staining intensity was greater than 100

matrix. Instead, an inflammatory environment is maintained with intense cell turnover, tissue remodeling, and cell migration, which leads to enhanced fibrosis, stiffness, erosion of adjacent organs, nerve entrapment, and pain. At least in some patients, this chronic process with the permanent activation of inflammatory immune cells can open the door for a systemic inflammatory response syndrome with subsequent complaints or even autoimmune diseases (Cohen Tervaert, 2018).

As a never healing process, the risks will accumulate over the years, questioning mesh utilization for young patients. Future attempts to improve the biocompatibility of meshes should focus on the reduction of the heterogeneous inflammatory infiltrate and the promotion of normal wound healing mechanisms.

Several limitations have to be considered. Our collection of explanted human mesh samples represents a selection of apparent mesh failures, often with insufficient knowledge about the various materials used, and with different intervals after implantation into non-healthy tissues. However, the current problem of meshes is the relation to some complications, and we have to understand why this happens. Many patients obviously can tolerate meshes without any problems, and it can be speculated that these patients may have a distinct immunological response. But at least in patients, who require a revision operation, the local inflammatory cells of the FBG revealed a complex pattern of activation. Future studies have to show, whether the downregulation of this inflammation is able to reduce the side effects and complications.

The indication for mesh explantation may affect the tissue reaction seen, whether the reason is recurrence, pain, or infection. In particularly any bacterial infection, either low or high grade is supposed to change the local tissue response. However, considering our experience with histopathological analysis of explanted meshes, we considered the meshes used in this study to be representative. Any larger sample size will hardly change the principal finding of substantial co-expression in CD68+ cells substantially. Due to the limited clinical data provided any meaningful correlation between outcome and the tissue response requires huge cohorts with a prospective data assessment. Additionally, to the many confounders given by the complex staining protocol, it is the location and size of the ROI of course that

TABLE 5 Evaluation of the proliferation within the inflammatory infiltrate of the foreign body granuloma.

	PP mesh (by mesh-sample) (n = 7)			PVDF mesh (by mesh-sample) (n = 5)		
Staining	Mean	Min	Max	Mean	Min	Max
CD68+	23.1	15.3	23.1	31.4	25.1	35.4
Ki67+	5.5	9.8	2.3	6.8	4.4	10.5
CD68 + Ki67+	3.1	4.9	1.3	4.0	2.2	6.3
CD68 + Ki67+/CD68+	12.9	8.5	20.9	12.4	6.6	17.8
CD68 + Ki67+/Ki67+	56.6	43.4	70.7	57.9	35.9	69.8

Note: Analysis of co-expression for CD68 + Ki67+, and co-expression in relation to either CD68+ or Ki67+ within the foreign body granuloma of human mesh explants. Data are presented in mean percentages of seven PP meshes and five PVDF meshes (11–18 regions of interest each). Positive cells have a mean staining intensity >100.

can affect the results. Extended inflammation with an ROI limited to the infiltrate of the FBG will lead to increased cell counts, whereas large ROIs that include wide areas of polymeric fibers, adjacent fat tissue, or excessive collagen deposits will show reduced numbers of nuclei. Correspondingly, the percentage of co-expressing cells may be affected. Our choice of an ROI of 1 mm^2, which usually includes about 2,000–5,000 cells of the inflammatory infiltrate, covers most of the inflammatory infiltrate around a mesh fiber. Even if parts of the ROI include adjacent noninflammatory tissues, it is both the number of CD68+ cells and the number of cells being positively stained with a second marker, which are reduced. Subsequently, the percentage of co-expressing CD68+ cells remains widely constant, which therefore can serve as the robust but specific property of the mesh. The analysis of the staining intensity only in the area of the nuclei cannot exclude that despite thin sections of about 2 μm the positive staining might be based on some overlapping cytoplasm membrane, but it offers the option to define positively stained cells in an objective and reliable way. To assure ourselves that our method identified true co-expression, we applied a cut-off fluorescence value of 100. This approach ensured a high PPV, which provides us with the most confidence for true positive selection. However, in some cases, the use of a lower cut-off value could have been argued, which would lead to higher percentages of double and single "positive" cells, at the loss of objectivity. It should be noted that lowering this cut-off only supports the conclusions of this study.

ACKNOWLEDGMENTS

We gratefully thank A. Fiebeler for her advice and always-helpful critical comments. L.C.D is funded by the Wellcome Trust (grant no. 103973/Z/14/Z). The acquisition of the TissueGnostic system is sponsored by the Federal Ministry of Education and Research (FKZ 13GW0108B).

CONFLICT OF INTEREST

The support by the Federal Ministry of Education and Research (FKZ 13GW0108B) enabled the acquisition of the Tissue Gnostics system. A.D. as PhD student is an employee of the FEG. U.K. and B.K. had research projects and consulting fees in collaboration with the mesh manufacturers Ethicon and FEG; expert testimony at lawsuits concerned with pelvic floor meshes; mesh patients with FEG. The financial disclosures listed result from their expertise, and none of them have tried to influence any part of the work for this manuscript.

REFERENCES

Adamthwaite, D., & Cooley, M. A. (1994). CD8+ T-cell subsets defined by expression of CD45 isoforms differ in their capacity to produce IL-2, IFN-gamma and TNF-beta. *Immunology*, *81*(2), 253–260.

Bachour, Y., Verweij, S. P., Gibbs, S., Ket, J. C. F., Ritt, M., Niessen, F. B., & Mullender, M. G. (2018). The aetiopathogenesis of capsular contracture: A systematic review of the literature. *Journal of Plastic, Reconstructive & Aesthetic Surgery*, *71*(3), 307–317.

Baron, C. S., & van Oudenaarden, A. (2019). Unravelling cellular relationships during development and regeneration using genetic lineage tracing. *Nature Reviews Molecular Cell Biology*, *20*(12), 753–765.

Boettcher, S., & Manz, M. G. (2017). Regulation of inflammation- and infection-driven hematopoiesis. *Trends in Immunology*, *38*(5), 345–357.

Bracq, L., Xie, M., Lambele, M., Vu, L. T., Matz, J., Schmitt, A., … Bouchet, J. (2017). T cell-macrophage fusion triggers multinucleated giant cell formation for HIV-1 spreading. *Journal of Virology*.*91*(24), e01237-17–.

Bucala, R., Spiegel, L. A., Chesney, J., Hogan, M., & Cerami, A. (1994). Circulating fibrocytes define a new leukocyte subpopulation that mediates tissue repair. *Molecular Medicine*, *1*(1), 71–81.

Cavaillon, J. M. (2011). The historical milestones in the understanding of leukocyte biology initiated by Elie Metchnikoff. *Journal of Leukocyte Biology*, *90*(3), 413–424.

Cohen Tervaert, J. W. (2018). Autoinflammatory/autoimmunity syndrome induced by adjuvants (Shoenfeld's syndrome) in patients after a polypropylene mesh implantation. *Best Practice & Research Clinical Rheumatology*, *32*(4), 511–520.

Davies, L. C., Jenkins, S. J., Allen, J. E., & Taylor, P. R. (2013). Tissue-resident macrophages. *Nature Immunology*, *14*(10), 986–995.

Davies, L. C., & Taylor, P. R. (2015). Tissue-resident macrophages: Then and now. *Immunology*, *144*(4), 541–548.

Glazener, C. M., Breeman, S., Elders, A., Hemming, C., Cooper, K. G., Freeman, R. M., … Montgomery, I. (2017). Mesh, graft, or standard repair for women having primary transvaginal anterior or posterior compartment prolapse surgery: Two parallel-group, multicentre, randomised, controlled trials (PROSPECT). *Lancet*, *389*(10067), 381–392.

Guilliams, M., Ginhoux, F., Jakubzick, C., Naik, S. H., Onai, N., Schraml, B. U., … Yona, S. (2014). Dendritic cells, monocytes and macrophages: A unified nomenclature based on ontogeny. *Nature Reviews Immunology*, *14*(8), 571–578.

Hameed, A., Hruban, R. H., Gage, W., Pettis, G., & Fox, W. M., 3rd. (1994). Immunohistochemical expression of CD68 antigen in human peripheral blood T cells. *Human Pathology*, *25*(9), 872–876.

Heymann, F., von Trotha, K. T., Preisinger, C., Lynen-Jansen, P., Roeth, A. A., Geiger, M., … Luedde, T. (2019). Polypropylene mesh implantation for hernia repair causes myeloid cell-driven persistent inflammation. *JCI Insight*, *4*(2), e123862.

Jablonski, W., & Meyer, H. (1938). The occurrence of wandering cells in cultures of nervous tissue in vitro, and the changes in their form in various media. *Journal of Anatomy*, *73*(Pt 1), 130–134.

Klinge, U., Dietz, U., Fet, N., & Klosterhalfen, B. (2014). Characterisation of the cellular infiltrate in the foreign body granuloma of textile meshes with its impact on collagen deposition. *Hernia*, *18*(4), 571–578.

Klosterhalfen, B., & Klinge, U. (2013). Retrieval study at 623 human mesh explants made of polypropylene–impact of mesh class and indication for mesh removal on tissue reaction. *Journal of Biomedical Materials Research, Part B: Applied Biomaterials*, *101*(8), 1393–1399.

Krzyszczyk, P., Schloss, R., Palmer, A., & Berthiaume, F. (2018). The role of macrophages in acute and chronic wound healing and interventions to promote pro-wound healing phenotypes. *Frontiers in Physiology*, *9*, 419.

Kunisch, E., Fuhrmann, R., Roth, A., Winter, R., Lungershausen, W., & Kinne, R. W. (2004). Macrophage specificity of three anti-CD68 monoclonal antibodies (KP1, EBM11, and PGM1) widely used for immunohistochemistry and flow cytometry. *Annals of the Rheumatic Diseases*, *63*(7), 774–784.

Murray, P. J., Allen, J. E., Biswas, S. K., Fisher, E. A., Gilroy, D. W., Goerdt, S., … Lawrence, T. (2014). Macrophage activation and polarization: Nomenclature and experimental guidelines. *Immunity*, *41*(1), 14–20.

Nolfi, A. L., Brown, B. N., Liang, R., Palcsey, S. L., Bonidie, M. J., Abramowitch, S. D., & Moalli, P. A. (2016). Host response to synthetic mesh in women with mesh complications. *American Journal of Obstetrics and Gynecology*, *215*(2), 206 e1–206 e8.

Pilling, D., Fan, T., Huang, D., Kaul, B., & Gomer, R. H. (2009). Identification of markers that distinguish monocyte-derived fibrocytes from monocytes, macrophages, and fibroblasts. *PLoS One*, *4*(10), e7475.

Ruckerl, D., & Allen, J. E. (2014). Macrophage proliferation, provenance, and plasticity in macroparasite infection. *Immunological Reviews*, *262* (1), 113–133.

Tennyson, L., Rytel, M., Palcsey, S., Meyn, L., Liang, R., & Moalli, P. (2018). Characterization of the T cell response to polypropylene mesh in women with complications. *American Journal of Obstetrics and Gynecology*, *220*(2), 187.e1–187.e8.

Wang, M., Windgassen, D., & Papoutsakis, E. T. (2008). Comparative analysis of transcriptional profiling of CD3+, CD4+ and CD8+ T cells identifies novel immune response players in T-cell activation. *BMC Genomics*, *9*, 225.

Wu, Y., Wu, W., Wong, W. M., Ward, E., Thrasher, A. J., Goldblatt, D., … Gustafsson, K. (2009). Human gamma delta T cells: A lymphoid lineage cell capable of professional phagocytosis. *Journal of Immunology*, *183* (9), 5622–5629.

Yona, S., & Gordon, S. (2015). From the reticuloendothelial to mononuclear phagocyte system - The unaccounted years. *Frontiers in Immunology*, *6*, 328.

Zaynagetdinov, R., Sherrill, T. P., Kendall, P. L., Segal, B. H., Weller, K. P., Tighe, R. M., & Blackwell, T. S. (2013). Identification of myeloid cell subsets in murine lungs using flow cytometry. *American Journal of Respiratory Cell and Molecular Biology*, *49*(2), 180–189.

SUPPORTING INFORMATION

Additional supporting information may be found online in the Supporting Information section at the end of this article.

How to cite this article: Klinge U, Dievernich A, Tolba R, Klosterhalfen B, Davies L. CD68+ macrophages as crucial components of the foreign body reaction demonstrate an unconventional pattern of functional markers quantified by analysis with double fluorescence staining. *J Biomed Mater Res*. 2020;1–13. https://doi.org/10.1002/jbm.b.34639